

## Recycling of organic matter in Antarctic sediments: A transect through the polar front in the Southern Ocean (Indian Sector)

*Christophe Rabouille*

Centre des Faibles Radioactivités, Laboratoire Mixte CNRS-CEA, Ave. de la Terrasse, 91190 Gif sur Yvette, France

*Jean-Francois Gaillard*

Department of Civil Engineering, Northwestern University, 2145 Sheridan Rd., Evanston, Illinois 60208-3109

*Jean-Claude Relexans*

Laboratoire d'Océanographie Biologique, CNRS-URA 197, Université de Bordeaux 1, 33405 Talence Cedex, France

*Paul Tréguer and Marie-Anne Vincendeau*

Institut Universitaire Européen de la Mer, Université de Bretagne Occidentale, BP 809, F-29285 Brest Cédex, France

### Abstract

Sediments from the Polar Front Zone were sampled in the Indian Sector of the Antarctic Ocean as part of the French JGOFS expedition *Antares I*. The first porewater distributions of O<sub>2</sub> and NO<sub>3</sub><sup>-</sup> and organic carbon data in the solid phase in this part of the ocean were used to model the recycling of organic matter in sediments. The data are described by a model containing two types of degradable organic matter with distinct reactivities. We estimate that the reactivity of the most labile organic carbon is very close to that of fresh organic matter with an average C:N ratio of 7. We estimate that particulate organic carbon fluxes deposited at the sediment–water interface range between 0.2 and 0.8 mol C m<sup>-2</sup> y<sup>-1</sup>, with two peaks near the Polar Front and the Subantarctic Front. The flux of organic carbon deposited at the sediment–water interface is unusually high and represents ~10–20% of estimated primary production. From these findings, we conclude that production in the pelagic zone of this region is strongly linked to deposition and recycling in the sediment.

The processes leading to recycling and burial of particulate organic matter in marine sediments affect the global oceanic carbon cycle over geological timescales. The oxidation of organic matter is the driving reaction of early diagenesis (Bernier 1980). It is coupled directly to a suite of biogeochemical processes that influence atmospheric pCO<sub>2</sub> on climatic timescales, including denitrification (Christensen 1994; Altabet et al. 1995; Ganesham et al. 1995) and calcite dissolution (Archer and Maier-Raimer 1994; Broecker and Peng 1987). In the deep sea, the recycling of organic matter in sediments is related primarily to mineralization reactivity and rain rate to the sea floor. Other key parameters include concentration of oxygen in overlying waters, bioturbation of surface sediment, and changes in sedimentation rate (Emerson et al. 1985; Emerson and Hedges 1988; Hedges and

Keil 1995; Murray and Kuivila 1990; Rabouille and Gaillard 1991a). Recently, there has been renewed interest in carbon dynamics in the Southern Ocean (JGOFS, 1992) that is thought to have played a major role in the control of the last glacial cycle (Duplessy et al. 1996; Michel et al. 1995; Pichon et al. 1992; Waelbroeck et al. 1995). However, little is known about the recycling efficiency of early diagenetic processes in the sediments of the Southern Ocean (Rutgers van der Loeff 1990; Rutgers van der Loeff and Berger 1991; Schluter 1991; Suess et al. 1980).

The reactivity of natural organic matter is related to its decomposition stage, which is in turn related to its mean age (Westrich and Bernier 1984). Sedimentary organic matter encompasses a mixture of various pools with different reactivities. In deep-sea sediments, most of the estimated decomposition rates come from diagenetic models (Emerson and Hedges 1988 and references therein) because organic matter abundance is low and rates vary slow. Various models for decomposition kinetics of sedimentary organic matter have been proposed (Boudreau and Ruddick 1990; Middelburg et al. 1993; Rabouille and Gaillard 1991b).

The flux of particulate matter on the sea floor generally reflects, over an oceanographic province, the magnitude of surface primary productivity. This flux was long thought to represent a very small fraction (<1%) of export production (Berger et al. 1989; Jørgensen 1983), leading to simple expressions for the rain rate of organic carbon as a function of water-column depth and surface productivity (Suess 1980).

### Acknowledgments

We thank the captain, officers, and crew of the *N. O. Marion-Dufresne* for their assistance in the cold of the Antarctic Ocean during coring operations. We also would like to acknowledge M. Taillefert for his help during the organic carbon analysis and P. Vessel and A. Goodliffe, who helped to prepare the map of the coring region using GMT software. D. Hoover and J. Love substantially improved the writing of this paper. We thank two anonymous reviewers for their thorough reviews and insightful comments. This work was supported by the Antarès program (JGOFS-Fr, INSU, and IFRTP), and the CEC Environment contract EV5V-CT92-0118. C.R. thanks SOEST (Univ. Hawaii) and Fred Mackenzie and his group for providing space and help during the writing of this paper. This is CFR contribution 1958.

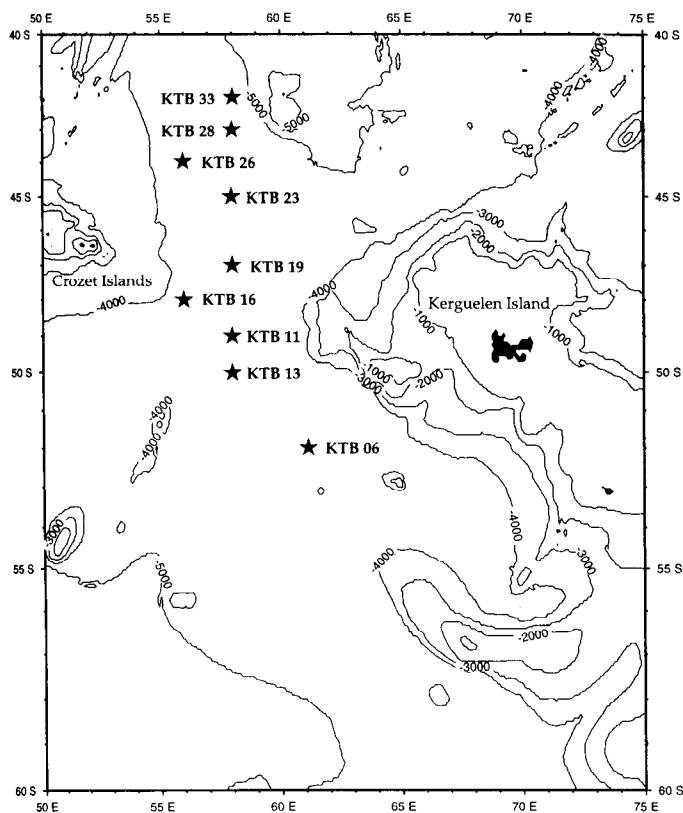


Fig. 1. Map showing the locations of the various coring sites.

Sediment trap studies have shown that there is a coupling between pelagic events and deep-sea floor deposition (Deuser and Ross 1980), and that relatively labile fractions of organic matter can be present at depth, packaged in fecal pellets or in rapidly sinking cell aggregates. Recent studies (Graf 1989; Lochte and Turley 1988; Smith et al. 1996; Thiel et al. 1988–1989; Turley and Lochte 1990) have shown that phytodetritus fluff layers are present in equatorial, temperate, and polar regions, showing that rapid transport of material from the ocean surface to the bottom can occur in many regions.

Table 1. A list of the different sampling sites and their position, water depth, and the relevant oceanographic zone according to front positions published in Belkin and Gordon (1996) (POOZ, Permanent Open Ocean Zone; PFZ, Polar Front Zone; SAFZ, Subantarctic Front Zone; STCZ, Subtropical Convergence Zone).

Zone	Core reference	Lat (S)	Long (E)	Depth (m)
POOZ	KTB06	–51°59	–61°08	4,710
PFZ	KTB13	–50°01	–57°59	4,600
PFZ	KTB11	–49°00	–57°59	4,395
PFZ	KTB16	–48°00	–56°00	4,240
PFZ	KTB19	–47°00	–58°00	4,590
SAFZ	KTB23	–45°00	–57°58	4,550
SAFZ	KTB26	–43°58	–55°58	4,460
SAFZ	KTB28	–43°00	–58°00	4,730
STCZ	KTB33	–42°00	–58°02	4,870

We herein report oxygen and nitrate distributions in pore water and organic carbon of surface sediments from the Indian Sector of the Southern Ocean along a transect across the Polar Front Zone. By using a diagenetic model with two types of degradable particulate organic matter (POM), we account for the observed variations of organic carbon, dissolved  $O_2$ , and  $NO_3^-$  in surficial sediments and make first estimates of (1) particulate organic matter reactivity in the Southern Ocean, and (2) integrated organic matter rain rates to the sea floor and their latitudinal variation across the Polar Front Zone. These results are compared to primary production to establish a link between surface production and organic matter deposition in the sediment.

## Methods

Samples were collected in April–May 1993 during the *Antares I* cruise of the *N. O. Marion-Dufresne* in the Crozet Island region of the Southern Indian Ocean (Fig. 1). Sediments were sampled primarily on a south–north transect from 52°S to 42°S, which extends over four different oceanographic zones: the Permanent Open Ocean Zone, the Polar Front Zone, the Subantarctic Front Zone, and the Subtropical Convergence Zone (see Table 1). Sediments in this region range from siliceous ooze in the south (90% of biogenic opal) to more terrigenous sediments north of 46°S (Rabouille et al. 1997).

Sediment cores were collected using a multicorer similar to that developed by Barnett et al. (1984), which permits retrieval of virtually undisturbed cores (60-mm i.d.) from 3,500- to 5,000-m depth. Once on deck, two separate cores were quickly removed from the supporting frame and capped. One of these cores was immediately extruded at 4°C and sliced every 0.5 cm in the top 4 cm (and every 1 cm afterwards). The sediments were transferred into Falcon centrifuge tubes, and the pore waters were extracted by 15 min of centrifugation at 4,500 rpm. The temperature inside the refrigerated centrifuge (Heraeus Minifuge 1.0) was maintained at 2°C. The supernatant was carefully removed using plastic syringes and filtered with 0.45- $\mu$ m Minisart Sartorius filters. Porewater aliquots were preserved in 5-ml tubes at 2°C until analysis. The sediments remaining after centrifugation were frozen immediately after core processing and kept frozen until further analysis in the home laboratory. The entire operation was completed within 4 h after retrieval of the cores.

The second core was utilized for oxygen measurements as described in De Wit et al. (1997). Porewater oxygen profiles were measured at in situ temperatures using a needle-style polarographic oxygen sensor (POS). Calibration was performed by measuring the oxygen content of stagnant overlying water by Winkler titration. Zero oxygen response was determined on a seawater sample with  $Na_2SO_3$  added. The  $O_2$  probes are useful for determining oxygen distribution over a depth of 10 cm in the sediment without disturbance. Measurement bias can be corrected by accounting for the change in porosity (De Wit et al. 1997).

Dissolved nitrate plus nitrite concentrations were determined on board by segmented flow colorimetry using a Technicon Auto-Analyzer II. The analysis was conducted ei-

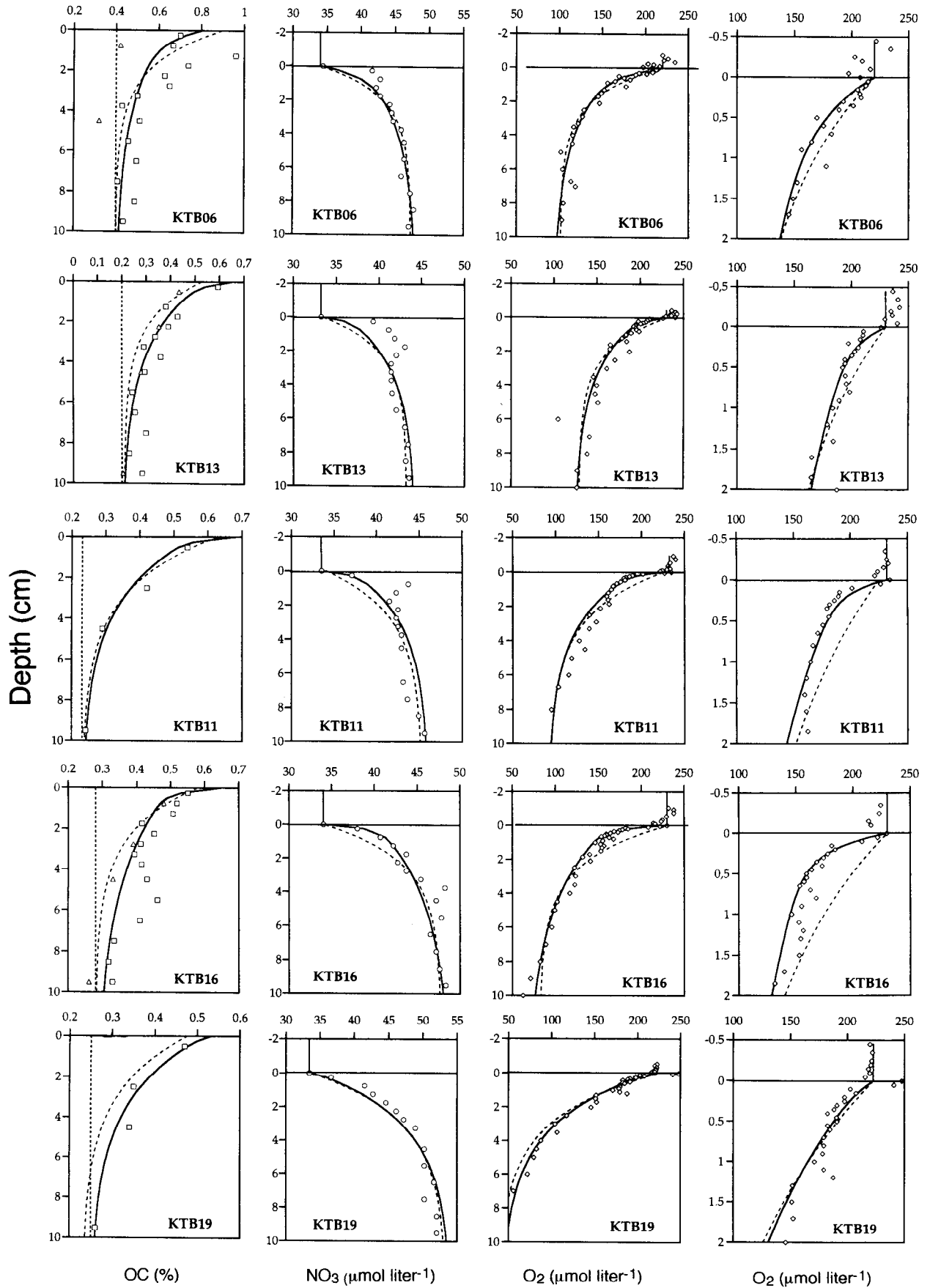


Fig. 2.

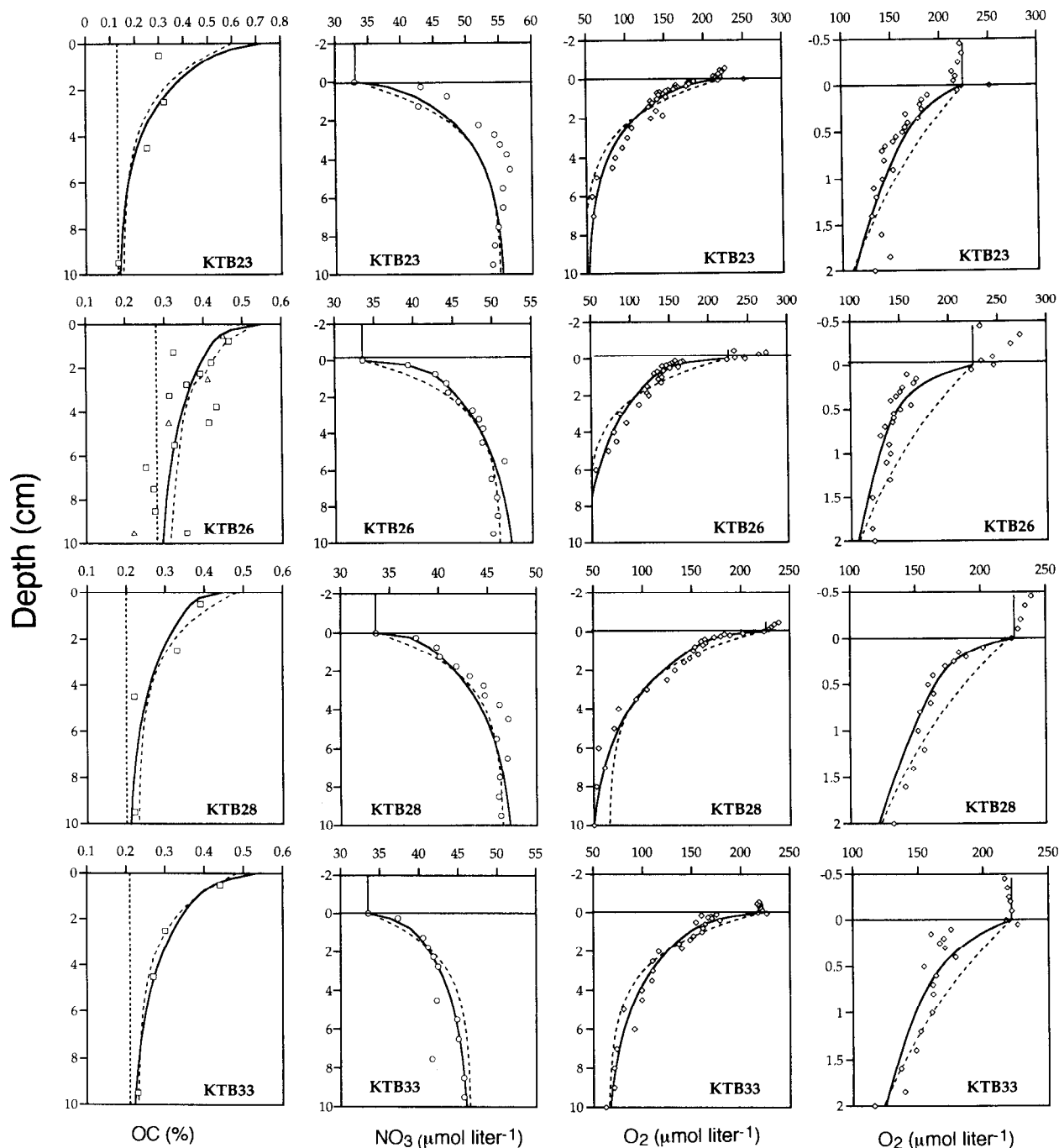


Fig. 2. Plots of OC, NO<sub>3</sub><sup>-</sup>, and O<sub>2</sub> for the nine sites sampled in this study. The dashed straight line on OC plots represents the model concentration of inert OC. The values obtained by the method of Cauwet et al. (1990) are shown as triangles; values obtained using the method of Verardo et al. (1990) are shown as squares. For the oxygen and nitrate plots, the flat part of the curve above the sediment-water interface represents deep-water values (measured 10 m above bottom). Note that there are two different depth and concentration scales for oxygen. Model curves: —, 2-G model; ---, 1-G model.

ther immediately after sampling or within 1 d after collecting the cores. Reproducibility of these analyses was >2%.

In the laboratory, organic carbon content of solids was determined on separate cores by using one of the two methods. The first method consists of analyzing the organic carbon in weighed dry sediment by combustion in a LECO CS 125 analyzer after acidification with 2 N HCl to remove

carbonates (Cauwet et al. 1990). At selected sites, a second method was used in which carbonates were removed with sulfurous acid and POC was determined by using flash combustion analysis with a Carlo-Erba CHN analyzer (Verardo et al. 1990). The reproducibility of this method is 10% for these particular samples; the LECO-derived values exhibit a reproducibility of 5%.

## Results

**Organic carbon**—Organic carbon in the solid phase ranges from 0.6–0.8% dry weight at the sediment–water interface to 0.2–0.3% at depth in the sediment (Fig. 2). Profiles exhibit strong gradients in the top 5 cm and a relatively constant concentrations thereafter. Individual profiles display some scatter, primarily due to the flocculent nature of dry sediments, which are dominated by a very porous siliceous fraction. This complicated the analysis of organic carbon and contributed to the low reproducibility of the flash combustion method. The scatter also adds uncertainty to the estimated kinetic parameters. However, qualitative agreement between the two different methods performed on different cores of the same multicorer is satisfactory and gives some constraints on the small-scale heterogeneity encountered in this area. The concentrations of carbon encountered at depth throughout the transect showed an average of 0.25% with a standard deviation of 0.05%. This is likely to represent POC that is essentially inert on timescales of centuries.

**Nitrate**—In the first 10 cm of the sediment, nitrate accumulates in pore water (Fig. 2) from decomposition of organic matter producing ammonium and primary amines that are then oxidized to nitrite, and from nitrate produced by nitrifying bacteria (Billen 1982; Suess et al. 1980). Bottom-water values are in the range previously obtained for Antarctic bottom water (Weiss et al. 1983), decreasing gradually from 34.4 to 33.5  $\mu\text{mol liter}^{-1}$  when moving from south to north. Nitrate concentrations at 10-cm depth were as high as 54  $\mu\text{mol liter}^{-1}$ , with concentrations averaging 48  $\mu\text{mol liter}^{-1}$ . These values are consistent with completely oxic sediments, in which nitrification is the major process shaping the nitrate profile.

**Oxygen**—Bottom-water concentrations of oxygen are in the expected range for Antarctic bottom water of the Enderby basin, ranging from 235  $\mu\text{mol liter}^{-1}$  in the south to 220  $\mu\text{mol liter}^{-1}$  north of the Polar Front. These concentrations compare fairly well with the GEOSECS data for this region (Weiss et al. 1983).

On the decimeter depth scale (Fig. 2), the oxygen profiles display the classical continuous exponential decrease expected for this type of open-ocean sediment, consistent with the primarily aerobic mineralization of the POM. The electrode is limited to 10 cm in reach, and concentrations at this depth for the different cores range from 40 to 135  $\mu\text{mol liter}^{-1}$ .

On a centimeter depth scale, oxygen profiles displayed a stronger decrease near the sediment–water interface than was observed on the 10-cm scale (with a typical e-folding depth of 0.3 vs. 2–3 cm for the 10-cm scale), thus indicating rapid consumption of oxygen near the sediment–water interface. The near-surface gradient is not likely to be an artefact due to sampling or storing of the core, and contamination by atmospheric oxygen penetrating through the water overlying the core during core recovery is minimal, since oxygen so measured is very similar (to within a few percent) to the oxygen concentrations measured on deep hydrocast (10–20 m above the bottom). Compression during penetration of the

core liner in the sediment can also be ruled out for two reasons. First, the magnitude of the gradient near the interface varies between cores extracted with the same sampler (e.g. core KTB06 has a less pronounced interfacial gradient but was sampled identically to the other cores). Second, samples obtained with the same corer in the tropical North Atlantic did not display any subcentimeter scale gradients near the interface, even though the sediments ranged from calcareous to organic rich (Gaillard unpubl. data).

## Discussion

With the present dataset, it is possible to address recycling and preservation of POM in these sediments. Assuming that early diagenesis is in steady state, we present a process model based on differential mass balances that allows estimation of benthic fluxes of POC, kinetics of POC decomposition, and C:N ratios of decomposing organic matter.

**Model for the oxic mineralization of POM**—The model presented here is a simplified version of that of Rabouille and Gaillard (1991b). In the Southern Ocean sediments that we studied, oxygen concentration at 10 cm never decreased below 40  $\mu\text{M}$ . Therefore, a description of aerobic processes with nonlimiting oxygen is appropriate. The reaction term of Rabouille and Gaillard (1991a) could be simplified from

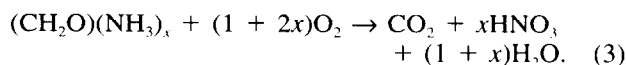
$$R_{\text{O}_2} = k_i OC_i \frac{\text{O}_2}{\text{O}_2 + K_m(\text{O}_2)} \quad (1)$$

to

$$R_{\text{O}_2} = k_i OC_i, \quad (2)$$

where  $R_{\text{O}_2}$  is the reaction term for oxygen consumption and organic carbon mineralization,  $OC_i$  is the concentration of organic carbon of type  $i$ ,  $K_m(\text{O}_2)$  is the half-saturation constant for oxygen utilization, and  $k_i$  is the kinetic constant for mineralization of  $OC_i$ .

A typical value for  $K_m(\text{O}_2)$  is generally on the order of 3  $\mu\text{M}$  (Rabouille and Gaillard 1991a). The net reaction of mineralization can be expressed by a simplified mass balance equation based on the stoichiometry of average POM:



This reaction allows for variable C:N ratios in the source material through the use of the variable  $x$  as a subscript and multiplier.

The reactivity of organic matter and its representation in models is still debated in the scientific literature. POM in sediments can be mineralized on very different timescales, from less than a month to millions of years (Canfield 1991; Emerson and Hedges 1988 and references therein; Toth and Lerman 1977). Therefore, when dealing with timescales ranging from seasons to a century, as in our study, a range of POM reactivities is expected (Middleburg et al. 1993). To represent this mixture of reactivities in mathematical models of early diagenesis, several approximations have been proposed: the multi-G model describes the behavior of several discrete classes of organic matter (Bernier 1980, 1982; Ham-

mond et al. 1996; Jørgensen 1978; Westrich et al. 1984); the time-dependent model (Middelburg 1989) depicts the reactivity of POM as a function of the time spent in the sediment; and the continuum model (Boudreau and Ruddick 1990) represents different classes of organic matter and their reactivities as a continuous function that varies as mineralization progresses. This latter formulation is probably the most realistic, but is difficult to incorporate into models containing bioturbation owing to the mathematical complexity.

For our cores, the double exponential shape of the oxygen profiles suggests that two classes of POM were being degraded with different mineralization rates: one rapidly degrading class (called labile) that caused the sharp gradient at the interface, and a more slowly degrading class of less labile POM (called hereafter intermediate) that accounted for the slow decrease.

To incorporate these two POM classes, we constructed a 2-G model in which each type of POM degraded with a first-order rate constant. For comparison purposes, we also constructed a 1-G model in which only one type of POM was degrading. The equations of this model are identical to those used in the 2-G model (Table 2) after simplifying for  $C_2$  of 0.

We also assumed constant porosity supported by porosity measurements (De Wit et al. 1997) and bioturbation over the modeled 10 cm of sediment, yielding the equations for  $OC$ ,  $O_2$ , and  $NO_3^-$  shown in Table 2. In these equations, the sedimentation transport was neglected, as is appropriate for the low Peclet number (0.02) calculated for low sedimentation rates typical of deep-sea sediments (Tromp et al. 1995). Because the sedimentation rates in this region might be higher than typical deep-sea values, we made sensitivity analysis on this parameter (*see sedimentation effects*).

**Determination of 2-G model parameters**—The model equations contain four state variable ( $O_2$ ,  $NO_3^-$ ,  $C_1$ , and  $C_2$ ) and 12 parameters (*see* Table 2 for definitions of terms). Some parameters are directly taken from the dataset ( $O_2$ (BW),  $NO_3^-$ (BW), average  $\phi$ ) or estimated ( $D_{O_2}$ ,  $D_{NO_3^-}$ ) from literature values (Broecker and Peng 1974; Himmelblau 1964; Li and Gregory 1974; Ullman and Aller 1982). The relationship between free water and sediment diffusion coefficient adopted in this study is  $D_s = D_{fs} \phi^{1.5}$ , and the free-water diffusion coefficient for oxygen and nitrate are taken to be 0.037 and 0.031  $m^2 yr^{-1}$ . From Eq. 3, we deduce that two of the parameters ( $\gamma_{O_2}$  and  $\gamma_{NO_3^-}$ ) are linked by a relationship in which

$$\gamma_{O_2} = 1 + 2 \gamma_{NO_3^-} \quad (4)$$

Therefore, six parameters ( $D_B$ ,  $k_1$ ,  $k_2$ ,  $\gamma_{NO_3^-}$ ,  $F_{C_1}$  and  $F_{C_2}$ ) remain to be determined by the model. It is possible to find an analytical solution to the set of equation (*see* Table 3). With our dataset, it is possible to determine independently the six quantities ( $x_1^*$ ,  $x_2^*$ ,  $\Delta C$ ,  $\Delta^1 O_2$ ,  $\Delta^2 O_2$ ,  $\Delta NO_3^-$ ) from the profiles, because of the two separate decreases in the oxygen profile. Therefore, the problem is fully determined, and a unique set of parameters can be determined with its associated uncertainty estimated to 25%.

**2-G model adjustment**—The dissolved oxygen, dissolved nitrate, and organic carbon profiles were fitted using the

Table 2. Equations and parameters of the 2-G model.

$D_B \frac{d^2 C_1}{dx^2} - k_1 C_1 = 0$
$D_B \frac{d^2 C_2}{dx^2} - k_2 C_2 = 0$
$\phi D_{O_2} \frac{d^2 O_2}{dx^2} - (1 - \phi) \gamma_{O_2} k_1 C_1 - (1 - \phi) \gamma_{O_2} k_2 C_2 = 0$
$\phi D_{NO_3^-} \frac{d^2 NO_3^-}{dx^2} + (1 - \phi) \gamma_{NO_3^-} k_1 C_1 + (1 - \phi) \gamma_{NO_3^-} k_2 C_2 = 0$
Boundary conditions:
at $x = 0$
$F_{C_1} = -(1 - \phi) D_B \frac{dC_1}{dx}$
$F_{C_2} = -(1 - \phi) D_B \frac{dC_2}{dx}$
$O_2 = O_2$ (BW)
$NO_3^- = NO_3^-$ (BW)
at $x \rightarrow \infty$
$\frac{dC_1}{dx} = \frac{dC_2}{dx} = \frac{dO_2}{dx} = \frac{dNO_3^-}{dx} = 0$

$C_1$ , labile organic C concn (mol $m^{-3}$ of solids)
$C_2$ , intermediate organic C concn (mol $m^{-3}$ of solids)
$O_2$ , oxygen dissolved in pore waters (mol $m^{-3}$ of water)
$NO_3^-$ , nitrate dissolved in pore waters (mol $m^{-3}$ of water)
$D_B$ , bioturbation coefficient ( $m^2 yr^{-1}$ )
$D_{O_2}$ , diffusion coefficient for oxygen in pore waters ( $m^2 yr^{-1}$ )
$D_{NO_3^-}$ , diffusion coefficient for nitrate in pore waters ( $m^2 yr^{-1}$ )
$\gamma_{O_2}$ , stoichiometric coefficient ( $O_2$ /Org C)
$\gamma_{NO_3^-}$ , stoichiometric coefficient ( $NO_3^-$ /Org C)
$k_1$ , kinetic constant for mineralization of labile organic matter ( $yr^{-1}$ )
$k_2$ , kinetic constant for mineralization of intermediate organic matter ( $yr^{-1}$ )
$O_2$ (BW), oxygen concentration in water overlying the sediment (mol $m^{-3}$ )
$NO_3^-$ (BW), nitrate concentration in water overlying the sediment (mol $m^{-3}$ )
$F_{C_1}$ , flux of labile POM to the sediment (mol C $m^{-2} yr^{-1}$ )
$F_{C_2}$ , flux of intermediate POM to the sediment (mol C $m^{-2} yr^{-1}$ )
$\phi$ , porosity
$x$ , depth (m)

equations shown in Table 3. The quantities  $x_1^*$ ,  $x_2^*$ ,  $\Delta C$ ,  $\Delta^1 O_2$ ,  $\Delta^2 O_2$ , and  $\Delta NO_3^-$  were determined from each of the measured profiles and used to calculate model parameters for each core. A 1-G model fit was performed as well for comparison to the 2-G model calculations. Figure 3 shows details of a representative set of concentration profiles obtained from the 2-G model (core KTB16). The model incorporates two types of reactive organic matter (labile and intermediate). The third type is assumed to be constant with depth and reflects the asymptotic concentration reached after degradation at the sediment–water interface. The labile POM has a shallow penetration depth (0.5 cm) and represents 25% of the total organic material at the sediment–water interface and 33% of the degradable organic material, although it constitutes 80% of the flux. The intermediate POM fraction penetrates more deeply (around 10 cm) and represents 33% of the total POM, 67% of the mineralized POM, and 20% of the flux. The inert fraction has the highest inventory in the

Table 3. Analytical solutions for OC, O<sub>2</sub>, and NO<sub>3</sub><sup>-</sup> profiles and observables quantities used to calculate the model parameters.

## 1. Solution to the equations for the 2-G model.

$$OC(x) = C_{\text{inert}} + C_1 + C_2 = C_{\text{inert}} + \frac{F_{C_1}}{(1-\phi)\sqrt{k_1 D_B}} \exp\left(-\sqrt{\frac{k_1}{D_B}} x\right) + \frac{F_{C_2}}{(1-\phi)\sqrt{k_2 D_B}} \exp\left(-\sqrt{\frac{k_2}{D_B}} x\right) \quad (1)$$

$$O_2(x) = O_2(\text{BW}) + \frac{\gamma_{O_2} F_{C_1}}{\phi D_{O_2}} \sqrt{\frac{D_B}{k_1}} \left[ \exp\left(-\sqrt{\frac{k_1}{D_B}} x\right) - 1 \right] + \frac{\gamma_{O_2} F_{C_2}}{\phi D_{O_2}} \sqrt{\frac{D_B}{k_2}} \left[ \exp\left(-\sqrt{\frac{k_2}{D_B}} x\right) - 1 \right] \quad (2)$$

$$NO_3^-(x) = NO_3^-(\text{BW}) - \frac{\gamma_{NO_3} F_{C_1}}{\phi D_{NO_3}} \sqrt{\frac{D_B}{k_1}} \left[ \exp\left(-\sqrt{\frac{k_1}{D_B}} x\right) - 1 \right] - \frac{\gamma_{NO_3} F_{C_2}}{\phi D_{NO_3}} \sqrt{\frac{D_B}{k_2}} \left[ \exp\left(-\sqrt{\frac{k_2}{D_B}} x\right) - 1 \right] \quad (3)$$

## 2. Observable quantities used to obtain model parameters

$$\begin{aligned} x_1^* &= \sqrt{\frac{D_B}{k_1}} & \Delta^1 O_2 &= \frac{\gamma_{O_2} F_{C_1}}{\phi D_{O_2}} \sqrt{\frac{D_B}{k_1}} \\ x_2^* &= \sqrt{\frac{D_B}{k_2}} & \Delta^2 O_2 &= \frac{\gamma_{O_2} F_{C_2}}{\phi D_{O_2}} \sqrt{\frac{D_B}{k_2}} \\ \Delta C &= \frac{F_{C_1}}{(1-\phi)\sqrt{k_1 D_B}} + \frac{F_{C_2}}{(1-\phi)\sqrt{k_2 D_B}} & \Delta NO_3^- &= \frac{\gamma_{NO_3}}{\phi D_{NO_3}} \left( F_{C_1} \sqrt{\frac{D_B}{k_1}} + F_{C_2} \sqrt{\frac{D_B}{k_2}} \right) \end{aligned}$$

$x_1^*$ , exponential constant for the first exponential decrease in oxygen (m)

$x_2^*$ , exponential constant for the second exponential decrease in oxygen (m)

$\Delta C$ , organic carbon concentration difference between 0 and 10 cm (mol m<sup>-3</sup> of solid)

$\Delta^1 O_2$ , oxygen concentration change over the first exponential decrease (mol m<sup>-3</sup> of pore water)

$\Delta^2 O_2$ , oxygen concentration change over the second exponential decrease (mol m<sup>-3</sup> of pore water)

$\Delta NO_3^-$ , nitrate concentration difference between 0 and 10 cm (mol m<sup>-3</sup> of pore water)

The model parameters  $F_{C_1}$ ,  $F_{C_2}$ ,  $k_2$ ,  $k_1$ ,  $D_B$ , and  $\gamma_{NO_3^-}$  can be computed from the above observable quantities using the following relationships:

$$\begin{aligned} F_{C_1} &= \frac{\phi D_{O_2} \Delta^1 O_2}{\gamma_{O_2} x_1^*} & D_B &= \frac{\phi D_{O_2} \Delta^{tot} O_2}{(1-\phi) \gamma_{O_2} \Delta C} & k_1 &= \frac{\phi D_{O_2} \Delta^{tot} O_2}{(1-\phi) \gamma_{O_2} \Delta C x_1^{*2}} \\ F_{C_2} &= \frac{\phi D_{O_2} \Delta^2 O_2}{\gamma_{O_2} x_2^*} & k_2 &= \frac{\phi D_{O_2} \Delta^{tot} O_2}{(1-\phi) \gamma_{O_2} \Delta C x_2^{*2}} & \gamma_{NO_3^-} &= \frac{D_{NO_3^-} \gamma_{O_2} \Delta NO_3^-}{D_{O_2} \Delta^{tot} O_2} \end{aligned}$$

where  $\Delta^{tot} O_2$  is the oxygen concentration difference between 0 and 10 cm ( $\Delta^1 O_2 + \Delta^2 O_2$ ).

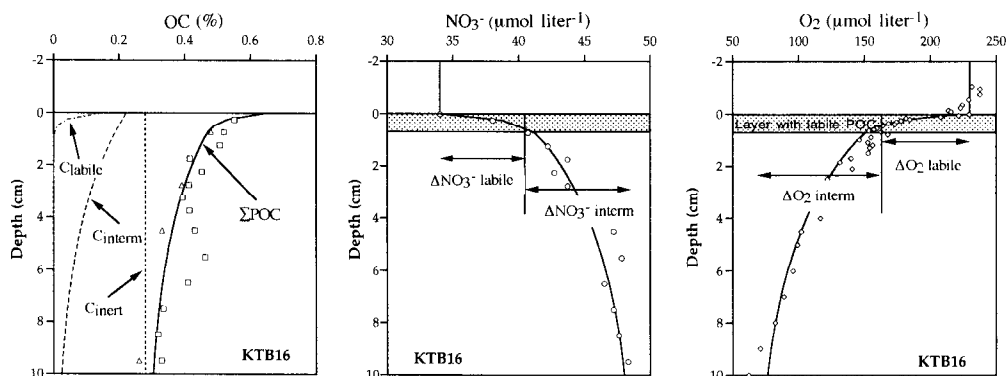


Fig. 3. Detailed 2-G model profiles for OC, oxygen and nitrate in core KTB16. The shadowed region corresponds to the layer where the labile fraction of the POM is degrading. The  $\Delta$ s refer to concentration changes associated with mineralization of the labile and intermediate reactivity POM fractions.

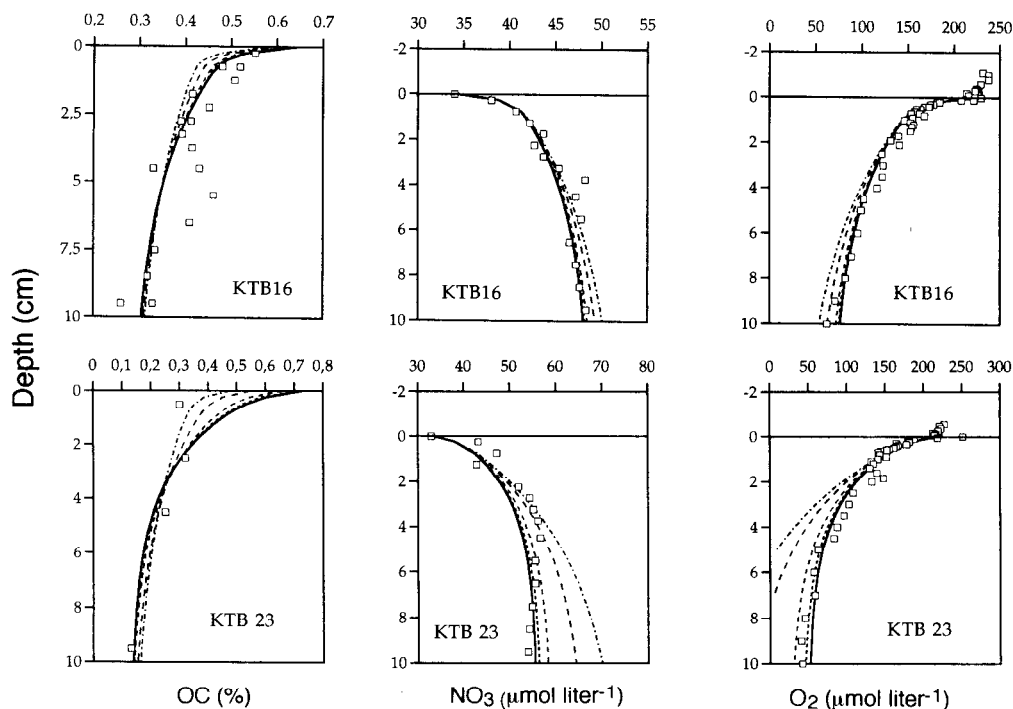


Fig. 4. Effects of increasing sedimentation rate (0–50 cm kyr<sup>-1</sup>) on O<sub>2</sub>, NO<sub>3</sub><sup>-</sup>, and OC profiles for two cores representing end members for transport processes. Other model parameters were kept constant for these simulations. □, data; —, 0 cm kyr<sup>-1</sup>; ·····, 3 cm kyr<sup>-1</sup>; - - -, 10 cm kyr<sup>-1</sup>; - · - ·, 30 cm kyr<sup>-1</sup>; - · - · ·, 50 cm kyr<sup>-1</sup>.

sediment and represents the largest fraction (40%) of the total POM, although its flux is two orders of magnitude smaller than the flux of the other fractions. Oxygen and nitrate profiles display large concentration gradients in the surface layer (Fig. 3) containing labile organic carbon, accounting for more than one-third of the total variation in their concentrations. It is noteworthy, however, that although the intermediate POM is less reactive, its mineralization produces the largest changes in nitrate and oxygen concentrations, because its concentration and penetration in the sediment are both larger, resulting in a more significant effect on porewater composition.

Figure 2 shows that the 2-G model fits the data better for the small-scale oxygen profile, organic carbon, and nitrate. The only profiles that do not show significant differences between the 1-G and the 2-G model are the ones obtained for core KTB06. This core, which was sampled in the middle of the POOZ, shows little evidence for the presence of more reactive POM. This may be related to the predominantly open ocean conditions at this site compared to the other sites.

Overall agreement between the 2-G model and the oxygen, organic carbon, and nitrate data is good. Because the modeled e-folding depths are the same for each of the three constituents (Eq. 1–3 of Table 3), we expect to see similar gradients in each of the three profiles. This is generally the case, except for the occurrence of very high nitrate gradients at the sediment–water interface in cores KTB06, KTB13, and KTB23. In these profiles, nitrate concentrations jump from 33–35 μmol liter<sup>-1</sup> in the overlying water to 38–44 μmol liter<sup>-1</sup> in the first sediment layer (0–0.5 cm). Model

fits are relatively poor for these cores, because the modeled concentration gradients due to the degradation of the most labile type of organic matter are not large enough to reproduce observed values. The large gradient below the sediment–water interface could be due to the “nitrate artifact” (Berelson et al. 1990; Martin and Sayles 1996), which could bias the nitrate determination near the interface due to ammonium accumulation and nitrification during core recovery and decompression. In our study, the time between recovery of the core and the end of centrifugation of the top core (first 4 cm) was ~2 h, which would minimize, but not avoid, the nitrate bias near the core top.

**Sedimentation effects**—We assessed the effects of sedimentation rate on modeled profiles by performing sensitivity tests on two datasets (KTB16 and KTB23) that represent the siliceous ooze region with a high bioturbation rate and the more terrigenous region with lower bioturbation rate. We calculated profiles of OC, oxygen, and nitrate for sedimentation rates of 0, 3, 10, 30, and 50 cm kyr<sup>-1</sup> (Fig. 4) while keeping the other parameters constant. The difference is small between profiles with no sedimentation and profiles calculated for a sedimentation rate of ≤10 cm kyr<sup>-1</sup>. For higher sedimentation rates (30–50 cm kyr<sup>-1</sup>), the difference is significant for core KTB23 but remains small for KTB16.

The sedimentation rate in the southern end of the transect is ~10 cm kyr<sup>-1</sup> and <5 cm kyr<sup>-1</sup> north of 45°N (J.-L. Reyss unpubl. data), which is in good agreement with values from Bareille (1991). Therefore, sedimentation transport is negligible.

Table 4. The nitrogen content of POM and its integrated nitrification rate as estimated by the model.  $(C:N)_{total}$  is the value obtained assuming a single C:N ratio for both fractions.  $(C:N)_{labile}$  refers to the ratio calculated in the first centimeter of the sediment (see text for details).

	Lat. (°S)	$(C:N)_{total}$	$(C:N)_{labile}$
KTB06	52	9.1	7.1
KTB13	50	9.1	4.1
KTB11	49	12.5	5.4
KTB16	48	11.1	9.2
KTB19	47	8.3	4.3
KTB23	45	7.1	4.5
KTB26	44	10.0	9.4
KTB28	43	14.3	10.4
KTB33	42	12.5	9.8

*Nitrogen cycling*—The high concentration of nitrate in pore water (up to  $55 \mu\text{mol liter}^{-1}$ ) suggests that nitrification is the most important nitrogen cycling pathway. The atomic C:N ratio of degradable POM is

$$C:N = \frac{D_{O_2} \Delta O_2}{D_{NO_3} \Delta NO_3} - 2, \quad (5)$$

and calculated values are close to those obtained from deep-sea particulate matter (Honjo et al. 1982; Watson and Whitfield 1985; see Table 4). Note that the C:N ratios of total degradable POM differ from those of fresh POM (C:N of  $\sim 7$ ) because our POM pool contains both fresh and degraded material. We estimated the C:N ratio of the labile fraction by using nitrate and oxygen variations within the first centimeter only (Table 4). We consider these results to be tentative because nitrate profiles contain only two concentration values in this interval and might be biased by the decomposition artifact on nitrate profiles (Berelson et al. 1990; Martin and Sayles 1996). However, the results are in rather good agreement with expected C:N values for fresh organic matter displaying a mean of 7.1.

*Is the steady-state assumption valid?*—Finally, we address the validity of the steady-state assumption. Because mineralization half-lives for the labile material are on the order of a few months and strong seasonality characterizes the Southern Ocean, we might expect nonsteady-state conditions

in the sediment resulting from high POC rain rates following the spring bloom. Some work on deep-sea sediment and porewater dynamics suggested that variation of input fluxes would be damped out, producing little variation in the porewater composition and solute fluxes (Martin and Bender 1988; Sayles et al. 1994). The principal reason for this constancy is the assumption that bioturbation rates are too slow to bury newly deposited organic carbon to depth where porewater profiles would be affected, implying that only low-reactivity carbon is present at depth. This view has recently been challenged by the observation of rapid bioturbation rates associated with freshly deposited particles (Smith et al. 1993); direct observations of large changes in deep-sea porewater composition on seasonal timescales have also been made (Gehlen et al. 1997). If high seasonal rain rates of POC occur in the Polar Front and the material is mixed rapidly into sediments, then the short residence time of the labile constituent could produce temporal variations in porewater profiles. However, the lack of detailed information on the nature and magnitude of transport processes and the uncertainty of seasonal variation of particulate flux prevent us from coming to a firm conclusion.

*Benthic POC fluxes*—POM fluxes at the sediment-water interface were calculated with the mass balance model. These values correspond to the fluxes of degradable organic matter (i.e. labile + intermediate), which is only a few percent less than the total flux of organic matter (including refractory material). The estimated fluxes of degradable POM range between  $0.2$  and  $0.8 \text{ mol C m}^{-2} \text{ y}^{-1}$  (Table 5). At this time, very few POC deposition rates have been estimated for the Antarctic Ocean. In a study in the South Weddell Sea ( $70^\circ\text{S}$ , 4,000-m depth, an open ocean region), POC mineralization was estimated from microelectrode oxygen profiles to be  $\sim 0.06 \text{ mol C m}^{-2} \text{ yr}^{-1}$  (Schluter 1991). Rutgers van der Loeff and Berger (1991) indicated an increased flux of organic carbon deposited in the sediment near the Polar Front using porewater oxygen profiles and  $^{210}\text{Pb}_{ex}$  inventories, but gave no values.

We can compare our flux estimates with values obtained in other oceanic regions. Reported fluxes under the equatorial high productivity zone are consistently around  $0.3 \text{ mol C m}^{-2} \text{ yr}^{-1}$  (Hammond et al. 1996; Martin et al. 1991; Murray et al. 1990; Smith 1989), with values  $< 0.1 \text{ mol C}$

Table 5. Total degradable OC fluxes derived from the model and the fraction contributed by labile and intermediate organic matter. Bioturbation coefficients ( $D_b$ ) resulting from the model are also displayed.

	Lat. (°S)	POC flux ( $\text{mol C m}^{-2} \text{ yr}^{-1}$ )	POC flux ( $\text{mg m}^{-2} \text{ d}^{-1}$ )	Labile/total in the POM	$D_b$ ( $\text{cm}^2 \text{ yr}^{-1}$ )
KTB06	52	0.28	9.3	0.82	0.35
KTB13	50	0.35	11.6	0.83	0.21
KTB11	49	0.6	19.9	0.92	0.28
KTB16	48	0.76	25.0	0.94	0.33
KTB19	47	0.21	7.0	0.51	0.31
KTB23	45	0.33	10.8	0.76	0.08
KTB26	44	0.66	21.6	0.92	0.31
KTB28	43	0.64	21.0	0.89	0.28
KTB33	42	0.33	10.9	0.83	0.19

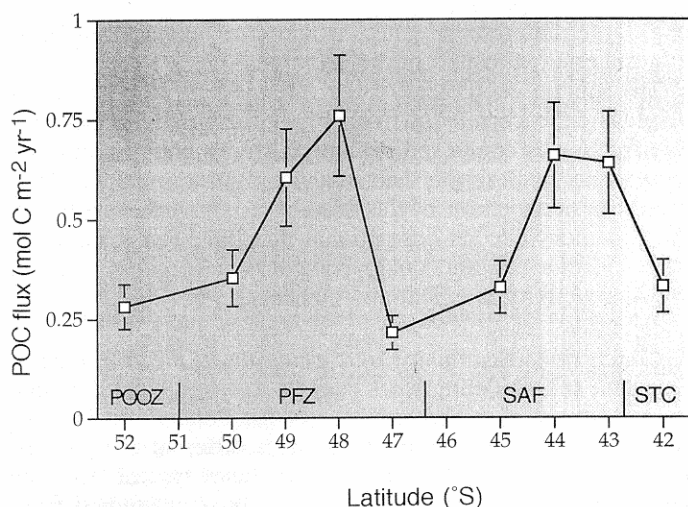


Fig. 5. Variation in POM flux vs. latitude. The two peaks at 49–48°S and 44–43°S corresponds to the Polar Front and the Subantarctic Front. Error bars of  $\pm 25\%$  are shown as a rough estimate of modeling uncertainty.

$\text{m}^{-2} \text{yr}^{-1}$  to the north and south. Similarly, in the tropical Atlantic and temperate Pacific, POC fluxes are higher near upwelling systems (Jahnke et al. 1989; Jahnke and Jackson 1987). For the North Pacific, fluxes as high as  $0.7 \text{ mol C m}^{-2} \text{yr}^{-1}$  have been reported for depths of  $\sim 4,000 \text{ m}$  (Jahnke and Jackson 1987).

When modeled POC fluxes are plotted against latitude, two distinct maxima are observed at 48–49°S and 43–44°S (Fig. 5). The region at 43–44°S is associated with the Subtropical Front where frontal processes may promote local upwelling and associated high export productivity, whereas the region at 48–49°S may be associated with the Antarctic Polar Front, which has been shown to be a site of elevated biomass in the Antarctic Ocean south of Africa (Luthjemars et al. 1985). Recent studies in the Bellingshausen Sea have shown that frontal activity in the Antarctic Ocean (67.5°S) may sustain both high biomass and productivity for periods of about a month (Boyd et al. 1995; Savidge et al. 1995). At this site, as at many other frontal systems, diatoms are prominent members of the phytoplankton assemblage, suggesting that rapid export may also be a common feature of frontal system in the Southern Ocean.

The partitioning of POM flux between the labile and intermediate fractions shows that most of the flux consists of labile material (Table 5); only one core (KTB19) departs from this pattern. The general dominance of the labile fraction suggests that, compared to other oceanic regimes, less degradation occurs in the water column.

Comparing the POC flux deposited at the sediment–water interface to productivity in the photic layer suggests that a large proportion of surface-water productivity is exported to the deep ocean. Productivity measurements are scarce and estimate that primary production in the Permanent Open Ocean Zone averages  $\sim 1\text{--}2 \text{ mol C m}^{-2} \text{yr}^{-1}$  (Holm-Hansen et al. 1977; Jacques 1989; Treguer and Van Bennekom 1991; Wefer and Fisher 1991) and  $\sim 5\text{--}7 \text{ mol C m}^{-2} \text{yr}^{-1}$  in the active region of the Polar Frontal Zone (Wefer and Fisher

Table 6. Degradation rates ( $k$ ) of labile and intermediate organic matter calculated from the 2-G model.

	Lat. (°S)	$k_{\text{labile}}$ (yr <sup>-1</sup> )	$k_{\text{interm}}$ (yr <sup>-1</sup> )
KTB06	52	1.4	0.028
KTB13	50	5.2	0.023
KTB11	49	7.8	0.015
KTB16	48	8.3	0.016
KTB19	47	13.9	0.035
KTB23	45	2.0	0.013
KTB26	44	7.7	0.019
KTB28	43	16.4	0.023
KTB33	42	2.1	0.015

1991). The mean of these two values ( $\sim 4 \text{ mol C m}^{-2} \text{yr}^{-1}$ ) indicates that 10–20% of primary production reaches the sea floor at an average water depth of 4,500 m, which would represent a strong coupling between pelagic production and deposition in the sediment. This is an unusually high value given the mean oceanic  $f$ -ratio (export/production) of 0.17 (Eppley 1989) and may be due to elevated export from the photic zone and minimal degradation during transport. High  $f$ -ratios (up to 0.6) have been observed in upwelling regions where large diatoms dominate the phytoplankton community. It has been shown that these diatoms can form aggregates and rapidly settle to the sea floor, particularly where pulses of primary production are decoupled from the growth of grazers (Alldredge and Gotschalk 1989). Continuous or pulsed export may also occur in frontal regions where nutrient inputs are enhanced through divergence, leading to conditions favorable for diatom growth and high  $f$ -ratios.

However, some caution is required with primary production data in this region, which has not been studied extensively either spatially nor temporally. As a result, we cannot rule out the possibility that average production values are substantially higher than  $4 \text{ mol C m}^{-2} \text{yr}^{-1}$  used here.

**Kinetics of POM mineralization**—Calculated degradation constants for the labile POM fraction provide additional support for rapid transport of exported production. First-order decay constants range between 1.4 and  $16 \text{ yr}^{-1}$ , resulting in residence times between 23 d and 8 months (Table 6).

These values are comparable to mineralization constants obtained for degrading microalgae in a number of studies. Degradation rates compiled by Emerson and Hedges (1988) show values  $>10 \text{ yr}^{-1}$  for the early stages of plankton degradation in seawater, with later stages characterized by kinetic constants of  $\sim 1\text{--}3 \text{ yr}^{-1}$  (Westrich and Berner 1984). More recent data collected on the degradation of organic fraction of diatoms (Harvey et al. 1995) and of Chl  $a$  from coastal phytoplankton (Sun et al. 1991) exhibit values ranging from 8 to  $33 \text{ yr}^{-1}$ . Thus, the kinetic constants calculated for the labile fraction in our 2-G model fall in the range reported for relatively fresh material.

The high POM degradation rates encountered at the sediment–water interface in our Antarctic samples indicate strong coupling between the photic production zone and the benthic region. Similar findings have been made in the Equatorial Pacific, where elevated kinetic constants for the labile

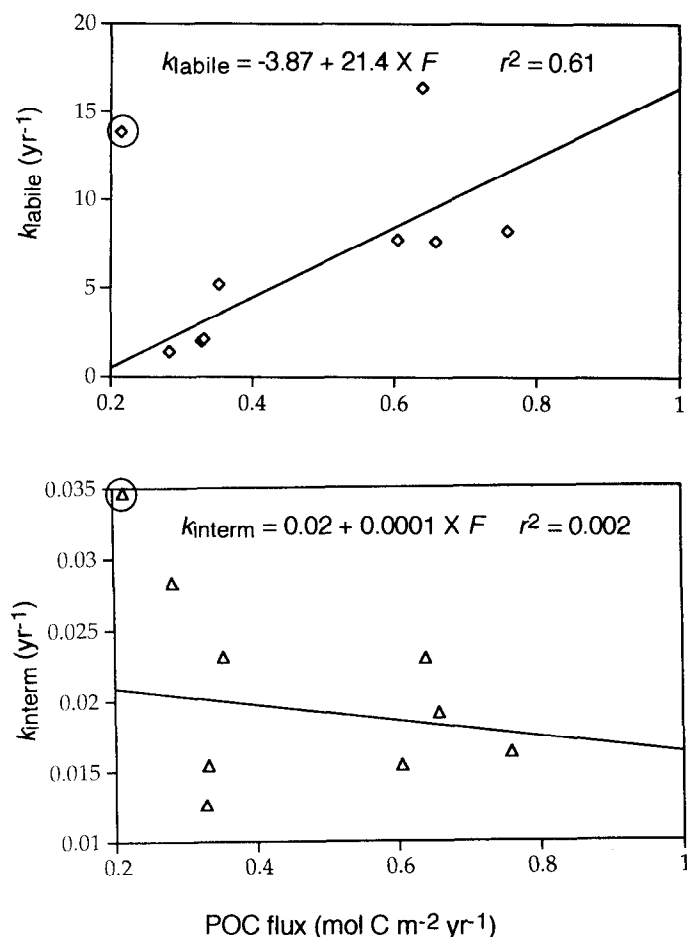


Fig. 6. Kinetic constants for the two types of organic matter (labile and intermediate) vs. the flux of POC. The equations shown are regressions that exclude the circled point (KTB19, see text for details). Coefficients of determination ( $r^2$ ) are also shown.

fraction (mean  $k = 15 \text{ yr}^{-1}$ ) were obtained by using a model comparable to ours (Hammond et al. 1996) at sites where phytodetritus was observed at the sea floor (Smith et al. 1996).

The kinetic constants calculated for the intermediate POM fraction ( $k = 0.013\text{--}0.035 \text{ yr}^{-1}$ ) are similar to values calculated for other open ocean sites (Grundmanis and Murray 1982; Murray and Kuivila 1990) and thus appear to be representative of the partially degraded organic material remaining after a few decades of degradation.

Degradation constants plotted vs. POC flux deposited at the sediment–water interface are shown in Fig. 6. A significant correlation is found between  $k_{labile}$  and POC flux but not between  $k_{interm}$  and POC flux. KTB19 is excluded from the regression analysis because the core is regarded as atypical in this dataset due to its unusually low labile fraction. This correlation indicates that greater particle fluxes correspond to less degradation in the water column. Indeed, bacterial degradation during settling removes the most reactive fractions of the organic matter, leaving less labile material for mineralization in the sediments. Therefore, a larger fraction of the total flux occurring as rapidly sinking material

(e.g. large diatom aggregates) would correspond to more labile material deposited in the sediment.

The kinetic coefficient of the intermediate POM fraction displays little correlation with POM flux, perhaps because this fraction is composed of material representing a number of seasonal cycles with their associated interannual variability (the residence time of this fraction is  $\sim 50 \text{ yr}$ ). As a result, the “memory” of its depositional flux has been lost. Alternatively, this material could constitute an organic fraction whose reactivity is essentially constant.

*Conclusion: Benthic–pelagic coupling in the Antarctic*—Our data and modeling work suggest that particulate organic matter deposited in the sediment of the Polar Front is composed of two different fractions with different reactivities. Degradation of the two fractions produces typical two-step decreases in all (but KTB19) oxygen profiles studied from the Polar Front and sharp gradients in nitrate just below the sediment–water interface. A model representing the two types of organic matter with their mineralization is able to reproduce satisfactorily the dataset.

Model results suggest that elevated fluxes of POM are deposited at the sediment–water interface (up to  $0.8 \text{ mol C m}^{-2} \text{ yr}^{-1}$ ). Higher deposition regions are closely associated with active fronts (i.e. the Polar Front and the Subantarctic Front). When compared to literature values for primary production in Antarctic Ocean and other frontal regions, the flux deposited at the sediment–water interface represents an unusually elevated proportion of both the export flux and primary production. Model results suggest that up to 10–20% of the primary production reaches the sediment in the Polar Front region studied. This may represent as much as 70–100% of the export production. This finding is also supported by calculated mineralization rate constants for the most labile fraction of the material, which fall in the range of values previously reported for fresh algal remains ( $1\text{--}10 \text{ yr}^{-1}$ ). The calculated C:N ratio of the labile fraction is also very close to the average C:N of fresh plankton.

These results suggest that the link between production and benthic processes is very strong in this region. The lack of degradation of particles in the water column during their settling may be attributed to low temperatures that slow bacterial reactions, lack of nutrients fueling bacterial activity, or elevated settling velocities due to aggregate formation.

## References

- ALLDREDGE, A. L., AND C. C. GOTSCHALK. 1989. Direct observation of the mass flocculation of diatom blooms: Characteristics, settling velocities and formation of diatom aggregates. *Deep-Sea Res.* **36**: 159–171.
- ALTABET, M. A., R. FRANCOIS, D. W. MURRAY, AND W. L. PRELL. 1995. Climate-related variations in denitrification in the Arabian Sea from sediment <sup>15</sup>N/<sup>14</sup>N ratio. *Nature* **373**: 506–509.
- ARCHER, D., AND E. MAIER-RAIMER. 1994. Effect on deep-sea sedimentary calcite preservation on atmospheric CO<sub>2</sub> concentration. *Nature* **367**: 260–263.
- BAREILLE G. 1991. Flux sédimentaires: Paléoprodutivité et paléocirculation de l'océan austral au cours des 150.000 dernières années. Thesis, Université de Bordeaux I.
- BARNETT, P. R. O., J. WATSON, AND D. CONELLY. 1984. A multiple

- corer for taking virtually undisturbed samples from shelf, bathyal and abyssal sediments. *Oceanol. Acta* **7**: 257–263.
- BELKIN, I. M., AND A. L. GORDON. 1996. Southern Ocean fronts from the Greenwich meridian to Tasmania. *J. Geophys. Res.* **101**: 3675–3696.
- BERELSON, W. M., AND OTHERS. 1990. Benthic fluxes and pore water studies from sediments of the central equatorial Pacific: Nutrient diagenesis. *Geochim. Cosmochim. Acta* **54**: 3001–3012.
- BERGER, W. H., V. S. SMETACEK, AND G. WEFER. 1989. Ocean productivity and paleoproductivity—an overview, p. 1–34. *In* V. S. W. Berger and G. Wefer [eds.], *Productivity of the oceans: Present and past*. Wiley & Sons.
- BERNER, R. A. 1980. *Early diagenesis: A theoretical approach*. Princeton Univ. Press.
- . 1982. A rate model for organic decomposition during bacterial sulfate reduction in marine sediments, p. 35–44. *In* Biogéochimie de la matière organique à l'interface eau-sédiment marin. *Coll. Int. CNRS* **293**.
- BILLEN, G. 1982. An idealized model of nitrogen recycling in marine sediments. *Am. J. Sci.* **282**: 512–541.
- BOUDREAU, B. P., AND B. R. RUDDICK. 1990. On a reactive continuum representation of organic matter diagenesis. *Am. J. Sci.* **291**: 507–538.
- BOYD, P. W., C. ROBINSON, G. SAVIDGE, AND P. J. LEB. WILLIAMS. 1995. Water column and sea-ice primary production during austral spring in the Bellingshausen Sea. *Deep-Sea Res.* **42**: 1177–1200.
- BROECKER, W. S., AND T. H. PENG. 1974. Gas exchange rates between air and sea. *Tellus* **26**: 21–35.
- , AND ———. 1987. The role of CaCO<sub>3</sub> compensation in the glacial to interglacial atmospheric CO<sub>2</sub> change. *Global Biogeochem. Cycles* **1**: 15–29.
- CANFIELD, D. E. 1991. Sulfate reduction in deep-sea sediments. *Am. J. Sci.* **291**: 177–188.
- CAUWET, G., F. GADEL, M. DA SOUZA SIERRA, O. DONARD, AND M. EWALD. 1990. Contribution of the Rhône to organic carbon inputs to the northwestern Mediterranean Sea. *Cont. Shelf Res.* **10**: 1025–1037.
- CHRISTENSEN, J. P. 1994. Carbon export from continental shelves, denitrification and atmospheric carbon dioxide. *Cont. Shelf Res.* **14**: 547–576.
- DEUSER, W. G. AND E. H. ROSS. 1980. Seasonal change in the flux of organic carbon in the deep Sargasso Sea. *Nature* **283**: 364–365.
- DE WIT, R., J.-C. RELEXANS, T. BOUVIER, AND D. MORIARTY. 1997. Microbial respiration and diffusive oxygen uptake of deep-sea sediments in the Southern Ocean (*Antares 1* cruise). *Deep-Sea Res. II* **44**: 1053–1068.
- DUPLESSY, J. C., AND OTHERS. 1996. High latitude deep water sources during the last glacial maximum and the intensity of the global oceanic circulation, p. 445–460. *In* W. G. Berger, G. Siedler, and D. J. Webb [eds.], *The South Atlantic: Past and present*. Springer-Verlag.
- EMERSON, S., K. FISCHER, C. REIMERS, AND D. HEGGIE. 1985. Organic carbon dynamics and preservation in deep-sea sediments. *Deep-Sea Res.* **32**: 1–21.
- , AND J. I. HEDGES. 1988. Processes controlling the organic carbon content of open ocean sediments. *Paleoceanography* **3**: 621–634.
- EPPLEY, R. W. 1989. New production: History, methods, problems, p. 85–97. *In* W. H. Berger, V. S. Smetacek, and G. Wefer [eds.], *Productivity of the ocean: Present and past*. Wiley & Sons.
- GANESHAM, R. S., T. F. PEDERSEN, S. E. CALVERT, AND J. W. MURRAY. 1995. Large changes in oceanic nutrient inventories from glacial to interglacial periods. *Nature* **376**: 755–758.
- GEHLEN, M., C. RABOUILLE, L. D. GUIDI-GUILVARD, AND U. EZAT. 1997. Drastic changes in deep-sea sediment porewater composition induced by episodic input of organic matter. *Limnol. Oceanogr.* **42**: 980–986.
- GRAF, G. 1989. Benthic pelagic coupling in a deep-sea benthic community. *Nature* **341**: 437–439.
- GRUNDMANIS, V., AND J. W. MURRAY. 1982. Aerobic respiration in pelagic marine sediments. *Geochim. Cosmochim. Acta* **46**: 1101–1120.
- HAMMOND, D. E., J. MC MANUS, W. BERELSON, AND T. KILGORE. 1996. Early diagenesis in equatorial Pacific sediments: Stoichiometry and kinetics. *Deep-Sea Res. II* **43**: 1365–1413.
- HARVEY, H. R., J. H. TUTTLE, AND J. T. BELL. 1995. Kinetics of phytoplankton decay during simulated sedimentation: Changes in biochemical composition and microbial activity under anoxic and oxic conditions. *Geochim. Cosmochim. Acta* **59**: 3367–3377.
- HEDGES, J. I., AND R. G. KEIL. 1995. Sedimentary organic matter preservation: An assessment and speculative synthesis. *Mar. Chem.* **49**: 81–115.
- HIMMELBLAU, D. M. 1964. Diffusion of dissolved gases in liquids. *Chem. Rev.* **64**: 527–550.
- HOLM-HANSEN, O., S. Z. EL-SAYED, G. S. FRANCESCHINI, AND R. L. CUHEL. 1977. Primary production and factors controlling phytoplankton growth in the Southern Ocean, p. 11–50. *In* G. Llano [ed.], *Adaptation within the Antarctic ecosystems*. Smithsonian Institution.
- HONJO, S., S. J. MANGANINI, AND J. J. COLE. 1982. Sedimentation of biogenic matter in the deep ocean. *Deep-Sea Res.* **29**: 609–625.
- JACQUES, G. 1989. Primary production in the open Antarctic Ocean during the austral summer: A review. *Vie Milieu* **39**: 1–17.
- JAHNKE, R. A., S. R. EMERSON, C. E. REIMERS, J. SCHUFFERT, K. RUTTENBERG, AND D. ARCHER. 1989. Benthic recycling of biogenic debris in the eastern tropical Atlantic Ocean. *Geochim. Cosmochim. Acta* **53**: 2947–2960.
- , AND G. A. JACKSON. 1987. Role of sea floor organisms in oxygen consumption in the deep North Pacific Ocean. *Nature* **329**: 621–623.
- JGOFS. 1992. Southern Ocean Process Study. Report N. 16. U.S. Joint Global Ocean Flux Study. Woods Hole, Massachusetts.
- JØRGENSEN, B. B. 1978. A comparison of methods for the quantification of bacterial sulfate reduction in coastal marine sediments. II. Calculations from mathematical models. *Geomicrob. J.* **1**: 29–47.
- . 1983. Processes at the sediment–water interface, p. 477–515. *In* B. Bolin and R. Cook [eds.], *The major biogeochemical cycles and their interactions*. SCOPE.
- LI, Y.-H., AND S. GREGORY. 1974. Diffusion of ions in sea water and in deep-sea sediments. *Geochim. Cosmochim. Acta* **38**: 703–714.
- LOCHTE, K., AND C. M. TURLEY. 1988. Bacteria and cyanobacteria associated with phytodetritus in the deep sea. *Nature* **333**: 67–69.
- LUTHJEMARS, J. R. E., N. M. WALTERS, AND B. R. ALLANSON. 1985. Oceanic frontal systems and biological enhancement, p. 11–21. *In* W. R. Siegfried, P. R. Condyand, and R. M. Laws [eds.], *Antarctic nutrient cycles and food webs*. Springer-Verlag.
- MARTIN, W. R., AND M. L. BENDER. 1988. The variability of benthic fluxes and sedimentary remineralization rates in response to seasonally variable organic carbon rain rates in the deep sea: A modelling study. *Am. J. Sci.* **288**: 561–574.
- , ———, M. LEINEN, AND J. ORCHARDO. 1991. Benthic organic carbon degradation and biogenic silica dissolution in the central equatorial Pacific. *Deep-Sea Res.* **38**: 1481–1516.

- , AND F. L. SAYLES. 1996.  $\text{CaCO}_3$  dissolution in sediments of the Ceara Rise, western equatorial Atlantic. *Geochim. Cosmochim. Acta* **60**: 243–263.
- MICHEL, E., L. LABEYRIE, J. C. DUPLESSY, N. GORFTI, M. LABRACHERIE, AND J. L. TURON. 1995. Could deep subantarctic convection feed the world deep basins during the last glacial maximum? *Paleoceanography* **10**: 927–942.
- MIDDELBURG, J. J. 1989. A simple rate model for organic matter decomposition in marine sediments. *Geochim. Cosmochim. Acta* **53**: 1577–1581.
- , T. VLUG, AND F. J. VAN DER NAT. 1993. Organic matter mineralization in marine systems. *Global Planet. Change* **8**: 47–58.
- MURRAY, J. W., AND K. M. KUIVILA. 1990. Organic matter diagenesis in the northeast Pacific: Transition from red clay to suboxic hemipelagic sediments. *Deep-Sea Res.* **37**: 59–80.
- PICHON, J. J., L. D. LABEYRIE, G. BAREILLE, M. LABRACHERIE, J. DUPRAT, AND J. JOUZEL. 1992. Surface water temperature changes in the high latitudes of the southern hemisphere over the last glacial–interglacial cycle. *Paleoceanography* **7**: 289–318.
- RABOUILLE, C., AND J.-F. GAILLARD. 1991a. A model representing the deep-sea organic carbon mineralization and oxygen consumption in surficial sediments. *J. Geophys. Res.* **96**: 2761–2776.
- , AND ———. 1991b. Towards the EDGE: Early diagenetic global explanation. A model depicting the early diagenesis of organic matter,  $\text{O}_2$ ,  $\text{NO}_3$ , Mn, and  $\text{PO}_4$ . *Geochim. Cosmochim. Acta* **55**: 2511–2525.
- , ———, M.-A. VINCENTEAU, AND P. TREGUER. 1997. Biogenic silica recycling in surficial sediments across the Polar Front zone of the Southern Ocean (Indian Sector). *Deep-Sea Res. II* **44**: 1151–1176.
- RUTGERS VAN DER LOEFF, M. M. 1990. Oxygen in pore waters of deep-sea sediments. *Phil. Trans. Roy. Soc.* **331**: 69–84.
- , AND G. W. BERGER. 1991. Scavenging and particle flux: Seasonal and regional variations in the Southern Ocean (Atlantic sector). *Mar. Chem.* **35**: 553–568.
- SAVIDGE, G., D. HARBOUR, L. C. GILPIN, AND P. W. BOYD. 1995. Phytoplankton distributions and production in the Bellingshausen Sea, austral spring 1992. *Deep-Sea Res.* **42**: 1201–1224.
- SAYLES, F. L., W. R. MARTIN, AND W. G. DEUSER. 1994. Response of benthic oxygen demand to particulate organic carbon supply in the deep sea near Bermuda. *Nature* **371**: 686–689.
- SCHLUTER, M. 1991. Organic carbon flux and oxygen penetration into sediments of the Weddell sea: Indicators for regional differences in export production. *Mar. Chem.* **35**: 569–579.
- SMITH, C. R., D. J. HOOVER, S. E. DOAN, R. H. POPE, D. J. DEMASTER, F. C. DOBBS, AND M. A. ALTABET. 1996. Phytodetritus at the abyssal seafloor across  $10^\circ$  of latitude in the central equatorial Pacific. *Deep-Sea Res. II* **43**: 1309–1338.
- , R. H. POPE, D. J. DEMASTER, AND L. MAGAARD. 1993. Age-dependent mixing of deep-sea sediments. *Geochim. Cosmochim. Acta* **57**: 1473–1488.
- SMITH, K. L. J. 1989. Short time-series measurements of particulate organic carbon flux and sediment community oxygen consumption in the North Pacific. *Deep-Sea Res.* **36**: 1111–1119.
- SUESS, E. 1980. Particulate organic carbon flux in the oceans—surface productivity and oxygen utilization. *Nature* **288**: 260–263.
- , P. J. MULLER, H. S. POWELL, AND C. E. REIMERS. 1980. A closer look at nitrification in pelagic sediments. *Geochem. J.* **14**: 129–137.
- SUN, M. Y., R. A. ALLER, AND C. LEE. 1991. Early diagenesis of chlorophyll *a* in Long Island Sound sediments: A measure of carbon flux and particle reworking. *J. Mar. Res.* **49**: 379–401.
- THIEL, H., AND OTHERS. 1988–1989. Phytodetritus on the deep-sea floor in a central oceanic region of the northeast Atlantic. *Biol. Oceanogr.* **6**: 203–239.
- TOTH, D. J., AND A. LERMAN. 1977. Organic matter reactivity and sedimentation rates in the ocean. *Am. J. Sci.* **277**: 465–485.
- TREGUER, P., AND A. J. VAN BENNEKOM. 1991. The annual production of biogenic silica in the Antarctic Ocean. *Mar. Chem.* **35**: 477–487.
- TROMP, T. K., P. VAN CAPPELLEN, AND R. M. KEY. 1995. A global model for the early diagenesis of organic carbon and organic phosphorus in marine sediments. *Geochim. Cosmochim. Acta* **59**: 1259–1284.
- TURLEY, C. M., AND K. LOCHTE. 1990. Microbial response to the input of fresh detritus to the deep-sea bed. *Palaeogeogr. Palaeoclimatol. Palaeoecol.* **89**: 3–23.
- ULLMAN, W. J., AND R. C. ALLER. 1982. Diffusion coefficients in nearshore sediments. *Limnol. Oceanogr.* **27**: 552–556.
- VERARDO, D. J., P. N. FROELICH, AND A. MCINTYRE. 1990. Determination of organic carbon and nitrogen in marine sediments using the Carlo Erba NA-1500 analyser. *Deep-Sea Res.* **37**: 157–165.
- WAELEBROECK, C., AND OTHERS. 1995. Comparing the Vostok ice deuterium record and series from Southern Ocean core MD 88-770 over the last two glacial–interglacial cycles. *Climate Dynamics* **12**: 113–123.
- WATSON, A. J., AND M. WHITFIELD. 1985. Composition of particles in the global ocean. *Deep-Sea Res.* **32**: 1023–1039.
- WEFER, G., AND G. FISHER. 1991. Annual primary production and export flux in the Southern Ocean from sediment trap data. *Mar. Chem.* **35**: 597–613.
- WEISS, R. F., W. S. BROEKER, H. CRAIG, AND D. SPENCER. 1983. Geosecs Indian Ocean expedition: Hydrographic data. National Science Foundation.
- WESTRICH, J. T., AND R. A. BERNER. 1984. The role of sedimentary organic matter in bacterial sulfate reduction: The G-model tested. *Limnol. Oceanogr.* **29**: 236–249.

Received: 27 November 1996

Accepted: 24 June 1997